IEEE Access
Multidisciplinary ⋮ Rapid Review ⋮ Open Access Journal

Received February 21, 2022, accepted March 7, 2022, date of publication March 10, 2022, date of current version March 17, 2022.

Digital Object Identifier 10.1109/ACCESS.2022.3158567

A Coordinated Control Method for Integrated System of Wind Farm and Hydrogen Production: Kinetic Energy and Virtual Discharge Controls

KENTA KOIWA[1], (Member, IEEE), LINMAN CUI[1], TADANAO ZANMA[1], (Member, IEEE), KANG-ZHI LIU[1], (Senior Member, IEEE), AND JUNJI TAMURA[2], (Senior Member, IEEE)

[1]Department of Electrical and Electronic Engineering, Chiba University, Chiba 263-8522, Japan
[2]Department of Electrical and Electronic Engineering, Kitami Institute of Technology, Hokkaido 090-8507, Japan

Corresponding author: Kenta Koiwa (kenta.koiwa@chiba-u.jp)

ABSTRACT This paper proposes a novel coordinated control method of wind farms (WFs) and hydrogen production systems (HPSs). In a grid-connected system where the WF and the HPS are connected to the grid, the WF can supply the power to the grid, producing hydrogen in the HPS. Moreover, the output fluctuation of the WF can be mitigated when the HPS produces hydrogen from the output surplus. The purpose of the grid-connected system is to smooth the WF output fluctuation sufficiently, produce hydrogen constantly, and maintain a high capacity factor in the HPS. The proposed coordinated control achieves the mitigation of the WF output and the high capacity factor in the HPS. The key ideas are 1) utilizing the kinetic energy of wind generators and 2) virtual discharge of the HPS. The fluctuation components of the WF output are compensated by both the WF and the HPS. The proposed coordinated controller enables us to produce hydrogen constantly in the HPS with a low-rated power. The advantage of the proposed coordinated control is verified by a comparative analysis with conventional methods through simulations using real wind data.

INDEX TERMS Electrolyzer, output smoothing, hydrogen production, wind generation.

NOMENCLATURE

NOTATIONS OF WG AND WF

P	WG output.
P_{WF}	WF output.
$P^{\dagger}$	WG MPPT output reference.
$P^{\dagger}_{\mathrm{WF}}$	WF MPPT output reference.
$\Delta P^{\dagger}$	Fluctuation component of $P^{\dagger}_{\mathrm{WF}}$.
$\Delta\overline{P}_{\mathrm{WF}}$	Positive part of $\Delta P^{\dagger}$.
$\Delta\underline{P}_{\mathrm{WF}}$	Negative part of $\Delta P^{\dagger}$.
$P_{\mathrm{g}}(=P_{\mathrm{WF}}-P_{\mathrm{H}})$	Power supplied to grid.
$\hat{P}$	Captured wind power.
ρ (≈ 1.225 kg/m^3)	Radius of blade.
R	Air density.
V	Wind speed.
C_{p}	Power coefficient.
β	Blade pitch angle.
λ	Tip speed ratio.
ω	Rotor angular frequency.
H_{J} ($=3$ s)	Inertia constant.

NOTATIONS OF HPS

P_{H}	Power supplied to AC-DC converter.
$\hat{P}_{\mathrm{H}}$	Consumed power in HPS.
H [Nm^3/h]	Hydrogen gas flow rate.
η	Overall efficiency of converters.
V_{dc}	Output voltage in DC-DC converter.
I_{dc}	Output current in DC-DC converter.

SUBSCRIPTS

pu	Per-unit.
$i=1,2,\ldots,n$	Number of WG.

SUPERSCRIPTS

ref	Reference.
n	Rated value.

The associate editor coordinating the review of this manuscript and approving it for publication was Youngjin Kim.

I. INTRODUCTION

The penetration of renewable energy power generation (REPG) into power systems has rapidly grown due to the energy crisis, global warming, and other environmental problems. In particular, wind power generation has been widely used because it is clean, sustainable, and cost-effective

[1], [2]. However, the power system, including large-scale wind farms (WFs), faces degradation of the power quality such as frequency and voltage fluctuations because the WF outputs constantly fluctuate due to wind speed variations [3]–[5]. In the worst scenario, the supply-demand imbalance caused by the power fluctuation may lead to a power outage. Therefore, it is essential to mitigate the output fluctuation of the WFs [5]–[8]. To smooth the WF output, energy storage systems (ESSs) such as batteries have been investigated [5], [9], [10]. The ESS can mitigate the output fluctuation of the WF, and its charge/discharge efficiency is high. Nevertheless, it is difficult for an ESS to store the excess power of the WF for a long time due to the limited energy capacity of the ESS. In addition, an overperformance ESS is usually used since the rated power and the energy capacity of the ESS cannot be designed independently [11].

Nowadays, hydrogen is also spotlighted as an alternative source to fossil fuels because of environmental problems [2], [12]. Household and industrial fuel cells (FCs), fuel cell vehicles (FCVs), hydrogen powered heavy-duty trucks, and hydrogen stations for the FCVs have been developed as applications of hydrogen energy [2], [13]–[16]. Moreover, the hydrogen can be converted to other useful chemicals such as methane by blending the hydrogen with CO_2 [2]. Although hydrogen can be produced by reforming fossil fuels, the actual cause of the environmental problem is not solved through the conventional hydrogen production method. To overcome this problem, hydrogen production systems (HPSs) composed of electrolyzers (ELZs) have attracted attention [17], [18]. An ELZ produces hydrogen by water electrolysis, which is free from carbon dioxide using the power obtained with the REPG [1], [2]. The HPS is suitable for the absorption of surplus WF output for a long time since the hydrogen in the tank can easily be taken out, utilized, or transported at anytime. This property has a significant meaning, which is not found in the energy stored in the ESS, such as chemical energy in a battery and kinetic energy in a fly-wheel [19]. In addition, the rated power and the energy capacity of the HPS can be designed independently. Therefore, the HPS enables us to implement large-scale WFs, producing an alternative source to fossil fuels.

There exist two types of systems composed of the HPS and the REPG, such as the WF, i.e., stand-alone systems [20]–[23] and grid-connected systems [11], [12], [16], [24]–[30]. In the stand-alone system where the HPS and the WF are disconnected from the grid, hydrogen can be produced without considering the power quality in the power system. However, the stand-alone system has the disadvantage that the WF cannot supply its power to the grid. Namely, the WF cannot contribute directly to the power system.

In the grid-connected system where the WF and the HPS are connected to the grid, the WF can supply power to the grid while producing hydrogen in the HPS. Moreover, the output fluctuation of the WF can be mitigated when the HPS produces hydrogen by using the output surplus of the WF. Therefore, the grid-connected system is a key technology to successfully install large-scale WF in the grid and produce hydrogen simultaneously.

Specifically, the purpose of the grid-connected system is to smooth the WF output sufficiently, produce hydrogen constantly, and maintain a high capacity factor in the HPS. In [24]–[28], systems composed of WFs, HPSs, FCs, and energy storage systems (ESSs), such as a battery, were proposed. Moreover, some operation methods for the system were also investigated in [24]–[28]. In these methods, the combination of HPS and FC behaves like an ESS because the HPS produces hydrogen by consuming power, and the FC generates power by consuming hydrogen. However, a part of electrical and hydrogen energies is wasted when the hydrogen produced by the HPS is reconverted to the power in the FC to smooth the WF output [16]. In addition, if hydrogen is used in the FC in order to smooth the WF output, it is challenging to store hydrogen for applications such as FCVs. In [29], a cooperative operation method for the WF and the HPS based on Nash bargaining theory was proposed for a system composed of WFs and HPSs. The method can reduce the operation cost of the WF and the HPS. Nevertheless, mitigation of the WF output was not investigated. Smoothing control methods using HPS for the REPG, such as the WF and photovoltaics, were proposed in [11] [12], and [16]. These methods mitigate the output fluctuation of the WF without using the FC and the ESS. However, it is difficult to smooth the output fluctuation of the WF sufficiently because the HPS cannot discharge, unlike the FC and ESS. Moreover, a high-rated power of the HPS is required to consume the large output fluctuation. Since these methods only utilize the output fluctuation of the WF to produce hydrogen, the HPS is not able to produce hydrogen constantly even when the wind speed is constant. As a result, it is inevitable to lower the capacity factor in the HPS.

To the best of our knowledge, there exists no method for grid-connected systems composed of the WF and the HPS to smooth the WF output sufficiently and to produce hydrogen constantly, while keeping a high capacity factor in the HPS. This paper proposes a novel coordinated control method for the WF and the HPS. The proposed coordinated control achieves mitigation of the WF output fluctuation and high capacity factor in the HPS. The key ideas in the proposed coordinated control are 1) utilizing the kinetic energy (KE) of wind generators and 2) virtual discharge of the HPS. The fluctuation components of the WF output are divided into positive and negative parts and they are compensated by the WF and the HPS, respectively. The proposed coordinated controller enables us to produce hydrogen constantly in the HPS with a low-rated power. The advantage of the proposed coordinated control is verified by a comparative analysis with the methods proposed in [11], [12], and [16] through simulations.

The rest of this paper is organized as follows: Section II describes the system configuration and reviews the conventional control methods. We propose a coordinated control for

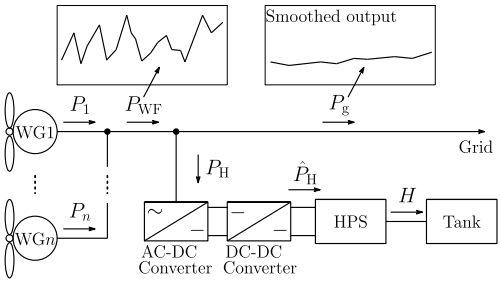

FIGURE 1. System configuration.

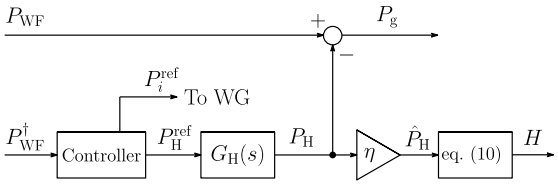

FIGURE 2. Block diagram of system.

the WF and the HPS in Section III. Section IV illustrates the effectiveness of the proposed method through scenario simulations with real wind data. Finally, we conclude this paper in Section V.

II. SYSTEM DESCRIPTION

This section reviews the system configuration composed of a WF and an HPS. For simplicity, a time function and its Laplace transform are denoted by the same notation, such as $P(t)$ and $P(s)$.

A. SYSTEM CONFIGURATION

Fig. 1 shows the system configuration, and Fig. 2 shows its block diagram. In Figs. 1 and 2, a wind generator (WG) comprises a variable speed wind turbine (VSWT), such as a permanent magnet synchronous generator. The HPS includes AC-DC and DC-DC converters. The notations and their meanings are listed in Nomenclature. The subscript pu in a variable denotes the per-unit of the variable and i ($i = 1, 2, \ldots, n$) corresponds to the number of the WG. For example, P_{ipu} denotes the per-unit power of the ith WG. The superscripts ref and n for a variable indicate the reference and the rated value, respectively. For example, P_H^{ref} and P_i^{n} denote the reference power for the AC-DC converter in the HPS and the rated power of the ith WG.

The role of the controller in Fig. 2 is to generate P_i^{ref} and P_H^{ref} to smooth the fluctuation of P_{WF}. The latter is also used for H. In Fig. 2, η is the overall efficiency of AC-DC and DC-DC converters, and $G_H(s)$ denotes the transfer function from P_H^{ref} to P_H. In this study, we assume that $G_H(s) \approx 1$ because the response speed of AC-DC and DC-DC converters is much faster [16], [20], and [26].

B. WIND TURBINE MODEL

The output characteristics of the WG are as follows [31]:

$$\hat{P}_i = \frac{1}{2}\rho\pi R^2 V_i^3 C_{pi}(\beta_i, \lambda_i), \tag{1}$$

$$C_{pi}(\lambda_i, \beta_i) = 0.5176\left(\frac{116}{\hat{\lambda}_i} - 0.4\beta_i - 5\right)e^{\frac{-21}{\hat{\lambda}_i}} + 0.0068\lambda_i, \tag{2}$$

$$\frac{1}{\hat{\lambda}_i} = \frac{1}{\lambda_i + 0.08\beta_i} - \frac{0.035}{\beta_i^3 + 1}, \tag{3}$$

$$\lambda_i = \frac{\omega_i R}{V_i}, \tag{4}$$

$$\omega_{ipu}\frac{d\omega_{ipu}}{dt} = \frac{1}{2H_J}\hat{P}_{ipu} - P_{ipu}. \tag{5}$$

In this paper, the dynamics of the back-to-back converter in the WG is ignored to shorten the simulation time, because it does not affect steady-state responses except transient responses, such as voltage dips. For this reason, we assume $P_i^{ref} \approx P_i$.

The VSWT can operate at a high efficiency because of the maximum power point tracking (MPPT) which keeps C_p maximum. We denote the maximum power coefficient and the optimum tip speed ratio as $C_p^{\dagger}$ and $\lambda^{\dagger}$, respectively. From a C_p-λ curve of the wind turbine in [31], we have $C_p^{\dagger} = 0.48$ and $\lambda^{\dagger} = 8.1$. Therefore, the MPPT output reference and its per-unit value are given by

$$P_i^{\dagger} = \frac{1}{2}\rho\pi R^2\left(\frac{R}{\lambda^{\dagger}}\right)^3 C_p^{\dagger}\omega_i^3, \tag{6}$$

$$P_{ipu}^{\dagger} = \frac{P_i^{\dagger}}{P^n} = \omega_{ipu}^3, \tag{7}$$

where P^n is calculated by $\frac{1}{2}\rho\pi R^2\left(\frac{R}{\lambda^{\dagger}}\right)^3 C_p^{\dagger}(\omega^n)^3$. From (7), when $P_i^{ref} = P_i^{\dagger}$, the MPPT can be achieved without measuring the wind speed. A pitch angle control system [32] is used to prevent the wind turbine from rotating faster than the rated speed.

C. ELECTROLYZER

In this section, we first review the ELZs for the REPG. Then, we explain the ELZ model used in this paper.

1) WATER ELECTROLYSIS SYSTEMS

In [33] and [34], the water electrolysis technologies were investigated in detail. This paragraph reviews the result briefly.

The hydrogen production systems are partitioned into three kinds of electrolysis systems: alkaline water electrolyzers (AWEs), solid oxide electrolyzer cells (SOECs), and proton exchange membrane electrolyzers (PEMEs) [33]. Table 1 summarizes their main advantages and disadvantages. The PEME has attracted much attention as one of the hydrogen production systems from the output of the REPG due to the

TABLE 1. Advantages and disadvantages of different water electrolysis technologies.

	AWE	SOEC	PEME
Advantages	Non-noble electro catalysts Low capital cost High durability	Non-noble electro catalysts High purity of gases (99.90%) Highest energy efficiency (90–100%)	Highest purity of gases (99.99%) High current density (0.6–2.0) High energy efficiency (80–90%) Compact design
Disadvantages	Low energy efficiency (70–80%) Low current densities (0.25–0.6 A/cm^2) Lowest purity of gases	Low durability High operational temperature Commercialization on a large scale	High cost of components Material corrosion under acidic environment Supply of pure water
Maturity	Commercial	Near commercial	Demonstration

advantages listed in Table 1 as well as a fast dynamic response when compared with the AWE and the SOEC [33], [35]. Due to these characteristics, we use an ELZ model based on the PEME in this paper.

2) ELECTROLYZER MODEL

In this subsection, we explain the ELZ model used in this paper. The notations for the ELZ are listed in Nomenclature. The ELZ is modeled as a diode, a resistor R_0, and an internal voltage E_0 under constant temperature and pressure [12], [18], as shown in Fig. 3. From Fig. 3 and Kirchhoff's voltage law, we have

$$I_{\mathrm{dc}} = \begin{cases} \frac{(V_{\mathrm{dc}} - E_0)}{R_0} & (V_{\mathrm{dc}} \geq E_0), \\ 0 & (V_{\mathrm{dc}} < E_0). \end{cases} \tag{8}$$

In this paper, we adopt the electrical model of [36] as the ELZ model. Fig. 4 shows the characteristics of a single ELZ module [36]. The module is comprised of 45 electrolytic cells, and its specification is listed in Table 2. From Fig. 4, we obtain a simplified model[1]:

$$H = \begin{cases} 0.019 I_{\mathrm{dc}} - 0.29 & (I_{\mathrm{dc}} > 15.264), \\ 0 & (I_{\mathrm{dc}} \leq 15.264). \end{cases} \tag{9}$$

From (8), (9), and $\eta P_{\mathrm{H}} = V_{\mathrm{dc}} I_{\mathrm{dc}} (= \hat{P}_{\mathrm{H}})$, H can be rewritten as follows[2]:

$$H = \begin{cases} H^{\dagger} & (H^{\dagger} \geq 0), \\ 0 & (H^{\dagger} < 0), \end{cases} \tag{10}$$

where

$$H^{\dagger} = 0.019 \left(\frac{-E_0 + \sqrt{E_0^2 + 4\eta R_0 P_{\mathrm{H}}}}{2R_0} \right) - 0.29. \tag{11}$$

Using (10) and (11), we can calculate H from P_{H} (See Appendix for a detailed calculation of $H^{\dagger}$).

An megawatt-scale HPS can be constructed by connecting modules of the ELZ in series and parallel [17], [20]. For instance, in the HPS which has four parallelized ELZ groups, each containing 28 cascaded ELZ modules, the rated power is about 5 MW, the rated gas flow rate is 840 Nm^3/h,

[1] The slope and y-intercept of the simplified model of H vs. I_{dc} in Fig. 4 are 0.019 and −0.29, respectively.

[2] From Fig. 2, $\hat{P}_{\mathrm{H}} = \eta P_{\mathrm{H}}$.

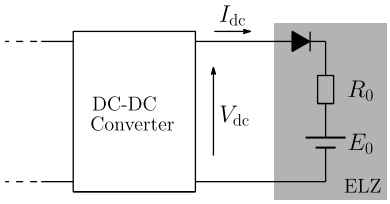

FIGURE 3. Electrical model of ELZ.

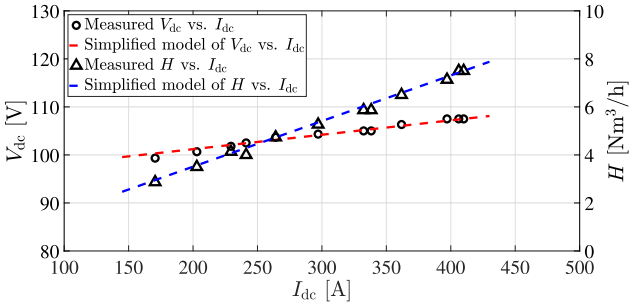

FIGURE 4. Characteristics of single ELZ module [36].

R_0 is 0.21 Ω, and E_0 is 2665.6 V. In addition, a larger-scale HPS can be achieved by connecting the megawatt-scale HPS, including AC-DC and DC-DC converters in parallel [11], [12]. For such an HPS, its total $H^{\dagger}$ becomes

$$H^{\dagger} = n_{\mathrm{h}} n_{\mathrm{s}} n_{\mathrm{p}} \left(0.019 \left(\frac{-E_0 + \sqrt{E_0^2 + 4\eta R_0 \left(\frac{P_{\mathrm{H}}}{n_{\mathrm{h}}} \right)}}{2R_0 n_{\mathrm{p}}} \right) - 0.29 \right), \tag{12}$$

where n_{s} is the number of cascaded ELZ modules in a group, n_{p} is the number of paralleled groups, and n_{h} is the number of HPSs connected in parallel. Note that $\left(\frac{P_{\mathrm{H}}}{n_{\mathrm{h}}} \right)$ in (12) denotes the consumed power in one of the megawatt-scale HPSs connected in parallel.

To evaluate the performance of the HPS, we define the capacity factor as

$$\text{Capacity factor} = \frac{\int_0^{\tau} H \, \mathrm{d}t}{\int_0^{\tau} H^{\mathrm{n}} \, \mathrm{d}t} \times 100\%, \tag{13}$$

where τ is the simulation period.

TABLE 2. Specification of one module of ELZ.

Rated power	44.075 kW
Rated voltage	107.5 V
Rated current	410 A
Rated gas flow rate	7.5 Nm^3/h
R_0	0.03 Ω
E_0	95.2 V

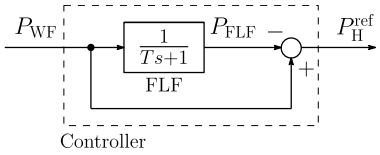

FIGURE 5. Standard FLF controller.

D. CONVENTIONAL SMOOTHING CONTROL USING HPS

This subsection briefly reviews a standard first-order low-pass filter (FLF) method and conventional methods proposed in [11], [12], and [16].

1) FLF

Fig. 5 shows the FLF controller [3], [5], [16]. In Fig. 5, P_{FLF} is the output of the FLF used as P_g^{ref}, and T is the time constant. The FLF controller has been widely used in ESS because of its simple structure. However, as shown in Fig. 6a, an HPS with an FLF controller cannot smooth P_{WF} sufficiently when $P_{FLF} > P_{WF}$ since it cannot discharge. This is different from the ESS which can discharge. In addition, the capacity factor of the HPS is low because the HPS hardly operates. As a result, hydrogen gas cannot be produced constantly.

2) METHOD PROPOSED IN [11] AND [12]

The FLF controller for the HPS was improved in [11] and [12]. In the method proposed in [11] and [12], P_g^{ref} and P_H^{ref} are given by

$$P_g^{ref} = P_{FLF} - P_\sigma, \tag{14}$$

$$P_H^{ref} = \begin{cases} P_{WF} - P_g^{ref} & (P_{WF} - P_g^{ref} \geq 0), \\ 0 & (P_{WF} - P_g^{ref} < 0), \end{cases} \tag{15}$$

where P_σ is the standard deviation of P_{WF} and it is given by

$$P_\sigma = \sqrt{\frac{\int_t^{t-T} (P_{WF} - P_{FLF})^2 dt}{T}}. \tag{16}$$

Figs. 6a and 6b show that the method proposed in [11] and [12] can smooth P_{WF} much better than the FLF controller. Nevertheless, P_{WF} cannot be mitigated sufficiently when $P_g^{ref} > P_{WF}$. Moreover, the capacity factor of the HPS is still low because the HPS cannot produce hydrogen when $P_g^{ref} > P_{WF}$ or $(P_{WF} - P_{FLF}) \approx 0$. It implies that hydrogen is not produced regardless of whether wind condition is good or not. In addition, as shown in 6b, the HPS with the high-rated power is required to compensate all fluctuation components of P_{WF}.

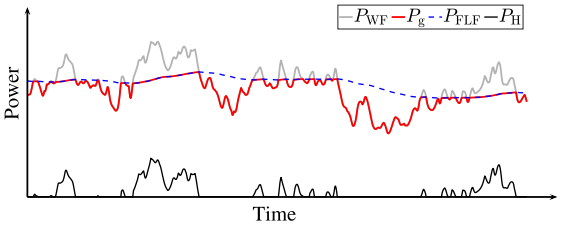

(a)FLF.

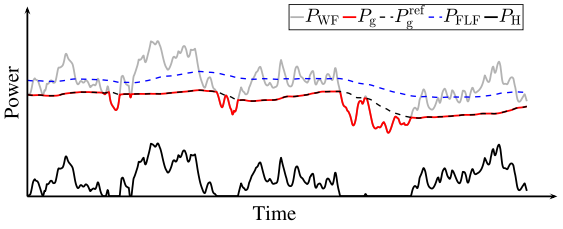

(b) Method proposed in [11], [12].

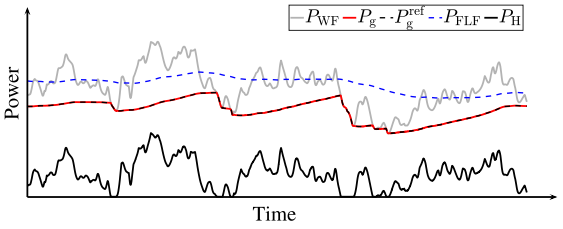

(c) Method proposed in [16]

FIGURE 6. Concept of conventional methods.

Note that it is assumed that the ELZ blocks in the HPS operate only at either $P_H^{ref} = P_H^n$ or $P_H^{ref} = 0$ in [11] and [12]. However, the HPS (ELZ) can operate at $0 \leq P_H^{ref} \leq P_H^n$. Therefore, for a fair comparison among methods for the HPS, we assume that the HPS controlled by the method proposed in [11] and [12] operates within $0 \leq P_H^{ref} \leq P_H^n$.

3) METHOD PROPOSED IN [16]

The FLF controller for the HPS was also improved in [16]. The basic concept of the method proposed in [16] is similar to the method proposed in [11] and [12]. In [16], the HPS operates based on

$$P_g^{ref} = \beta^\dagger(P_{WF}, P_{FLF}, T_w) \cdot P_{FLF}, \tag{17}$$

$$P_H^{ref} = P_{WF} - P_g^{ref}, \tag{18}$$

where $\beta^\dagger(P_{WF}, P_{FLF}, T_w)$ $(0 \leq \beta^\dagger \leq 1)$ is a gain used to modify P_{FLF}, and T_w is a buffer time. The calculation method of $\beta^\dagger$ is given in [16] and omitted in this paper. As shown in Fig. 6c, the method of [16] can smooth P_{WF} much more than the method of [11] and [12]. However, P_g obtained by this method includes fluctuation components, as compared with P_{FLF}. In particular, when P_{WF} suddenly decreases, P_g also decreases. It leads to the degradation of power quality in the power system. Moreover, it is difficult to produce hydrogen constantly and to reduce the rated power of HPS in the method

of [16] as well as the method of [11] and [12]. As a result, the decrease of the capacity factor in the HPS is inevitable.

In summary, there exists no method for the HPS, which can simultaneously smooth the output fluctuation of the WF sufficiently, produce hydrogen stably, and keep the capacity factor high.

III. COORDINATED CONTROL OF WF AND HPS

This section presents a novel coordinated controller for the WF and the HPS. The proposed coordinated controller is based on KE of the VSWT and virtual discharge of the HPS.

Kinetic energy control (KEC) for the VSWT has been widely investigated [37]–[39]. In the KEC, the KE is stored/released in the WG via rotor speed deceleration/acceleration so as to smooth the WG output. In other words, the WG does not operate based on MPPT. Nevertheless, the KEC cannot smooth the output fluctuation of the WF sufficiently because the available KE is low unlike the energy of ESS. In particular, excessive release of the KE may put a stop to the WG. Namely, it is not suitable to operate the WG in $P_i > P_i^\dagger$. In contrast, the operation in $P_i \le P_i^\dagger$ does not destabilize the WG because the pitch controller protects the WG even if ω_i is over 1 p.u.

As mentioned in Section II, it is difficult for the HPS to smooth the output fluctuation of the WF because the HPS cannot discharge, unlike ESS. In addition, hydrogen production in the HPS using fluctuation components of $P_{\rm WF}$ lowers the capacity factor of the HPS and requires a high-rated power of the HPS.

The proposed coordinated controller can overcome the problems in the KEC and the control of the HPS. In the proposed coordinated controller, the WF does not release the KE excessively. Specifically, the WF operates in $P_i \le P_i^\dagger$. Although the proposed KEC cannot remove all fluctuation components of the WF output, the HPS with the proposed controller compensates the residual fluctuation components. Therefore, the WF operates stably, and its output fluctuation can be mitigated sufficiently. In addition, since the HPS need not consume all fluctuation components of WF output, the HPS with a large-rated power is not required. This leads to an increase in the capacity factor in the HPS.

Fig. 7 shows the proposed coordinated controller. As mentioned before, the fluctuation of $P_{\rm WF}$ is smoothed by P_i and $P_{\rm H}$ whose references are generated by the proposed coordinated controller as $P_i^{\rm ref}$ and $P_{\rm H}^{\rm ref}$, respectively. Typical controllers regulate P_i to $P_i^{\rm ref}$ in the back-to-back converter of the WG, and $P_{\rm H}$ to $P_{\rm H}^{\rm ref}$ in the DC-DC converter of the HPS [12], [26]. The proposed coordinated controller consists of an FLF to extract the fluctuation component in $P_{\rm WF}^\dagger = \sum_{i=1}^n P_i^\dagger$, a KEC for the WF, and a virtual discharge control (VDC) for the HPS. In Fig. 7, $\Delta P_{\rm WF}$ is the fluctuation component of $P_{\rm WF}^\dagger$, $\Delta\overline{P}_{\rm WF} \ge 0$ and $\Delta\underline{P}_{\rm WF} \le 0$ are its positive and negative parts,[3] and $P_{\rm b} \ge 0$ is an offset value for the control of the HPS. As shown in Fig. 7, $\Delta\overline{P}_{\rm WF}$ and $\Delta\underline{P}_{\rm WF}$ are given by the limiters and they are compensated by the KEC and the VDC, respectively.

[3] $\Delta P_{\rm WF} = \Delta\overline{P}_{\rm WF} + \Delta\underline{P}_{\rm WF}$.

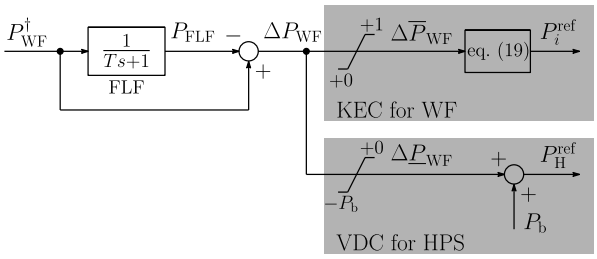

FIGURE 7. Proposed coordinated controller.

First, we present the KEC in Fig. 7. In the proposed KEC, the WGs operate based on

$$P_i^{\rm ref} = P_i^\dagger - \frac{P_i^\dagger}{P_{\rm WF}^\dagger}\Delta\overline{P}_{\rm WF}. \tag{19}$$

In (19), $\Delta\overline{P}_{\rm WF}$ is allocated to each WG by the second term of the right hand [39]. From (19), $P_i \approx P_i^{\rm ref}$ and $P_{\rm WF}^\dagger = \sum_{i=1}^n P_i^\dagger$, $P_{\rm WF}$ is given by

$$P_{\rm WF} = \sum_{i=1}^n P_i = P_{\rm WF}^\dagger - \Delta\overline{P}_{\rm WF}. \tag{20}$$

It is clear from (20) and Fig. 8a that $\Delta\overline{P}_{\rm WF}$ can be compensated by the proposed KEC. Since the proposed KEC compensates only $\Delta\overline{P}_{\rm WF}$, the WF does not release the KE excessively. In other words, the WGs operate based on MPPT when $P_{\rm WF}^\dagger \le P_{\rm FLF}$. Although it is inevitable to degrade the efficiency of the WG with the KEC, the operation based on the MPPT during $P_{\rm WF}^\dagger \le P_{\rm FLF}$ leads to efficiency improvement compared to an operation in which the KE is constantly used.

Next, we describe the proposed VDC for HPS. Although the HPS cannot discharge, the proposed VDC enables the HPS to discharge virtually. Therefore, the HPS with the proposed VDC can mitigate $\Delta\underline{P}_{\rm WF}$ (≤ 0). As shown in Fig. 7, $P_{\rm H}^{\rm ref}$ is given by

$$P_{\rm H}^{\rm ref} = P_{\rm b} + \Delta\underline{P}_{\rm WF}. \tag{21}$$

Note that $P_{\rm H}^{\rm ref} = 0$ when $(\Delta\underline{P}_{\rm WF} + P_{\rm b}) < 0$. From (20) and (21), $P_{\rm g}$ is given by

$$\begin{aligned} P_{\rm g} &= P_{\rm WF} - P_{\rm H} = P_{\rm WF}^\dagger - \Delta\overline{P}_{\rm WF} - \Delta\underline{P}_{\rm WF} - P_{\rm b} \\ &= P_{\rm FLF} - P_{\rm b}, \end{aligned} \tag{22}$$

where $P_{\rm FLF} = P_{\rm WF}^\dagger - \Delta P_{\rm WF}$ as shown in Fig. 7. A constant power, $P_{\rm b}$, is taken out from $P_{\rm FLF}$ and used for hydrogen production. From (22) and Fig. 8b, the HPS discharges $\Delta\underline{P}_{\rm WF}$ from the constant $P_{\rm b}$ supplied by the WF. As a result, smoothed power can be supplied to the grid.

The proposed coordinated controller cannot only smooth the WF output but also produce hydrogen constantly because the HPS operates around $P_{\rm b}$. In particular, when $P_{\rm b}$ is set

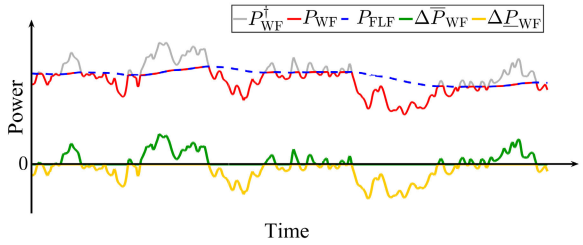

(a)WF output.

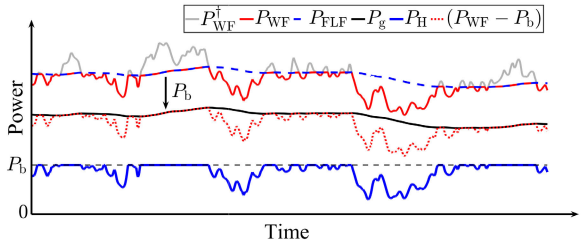

(b)Consumed power in HPS.

FIGURE 8. Concept of proposed coordinated controller.

to $P^{\mathrm{n}}_{\mathrm{H}}$, a high capacity factor of the HPS can be achieved. Although the HPS with the conventional controller cannot produce hydrogen when $\Delta P_{\mathrm{WF}} \approx 0$, the HPS with the proposed coordinated controller generates hydrogen in such a condition. Moreover, the rated power of the HPS can be designed to a small value since the HPS only compensates $\Delta\underline{P}_{\mathrm{WF}}$. It also leads to an increase in the capacity factor.

IV. SIMULATION VALIDATION

In this section, a comparative analysis is performed with the methods proposed in [11], [12], and [16] to validate the proposed coordinated controller through the simulations. We demonstrate the comparative analysis for a WF (500 MW) composed of five WG groups, and each group contains 20 WGs (5 MW/WG), assuming that WGs involved in each group operate under the same wind conditions [11], [40]. The evaluation is conducted based on a power ramp requirement in Japan [41]. The grid code is as follows:

- The maximum power change per five minutes is within 10% of the WF power rating.

The fluctuation ratio $\Delta F(x(t))$ in a five-minute window is defined as

$$\Delta F(x(t)) = \frac{\max\limits_{t-5\mathrm{min.}\le\tau\le t} x(\tau) - \min\limits_{t-5\mathrm{min.}\le\tau\le t} x(\tau)}{P^{\mathrm{n}}_{\mathrm{WF}}}, \quad (23)$$

where $x(t)$ is a signal such as $P_{\mathrm{g}}(t)$ and P_{WF}. From (23), the grid code is defined by

$$\Delta F(P_{\mathrm{g}}(t)) < 0.1. \quad (24)$$

The actual wind speed data[4] sampled every 3 s at a WF in Hokkaido, Japan, are used in the simulations. Fig. 9 shows

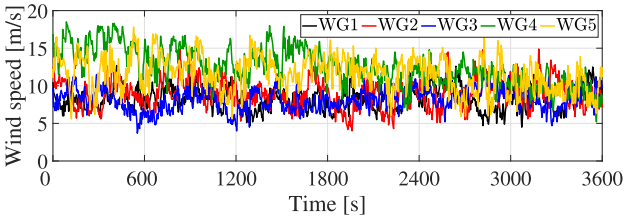

FIGURE 9. Wind speed (Scenario 1).

TABLE 3. Data of scenarios.

Scenario	1	2	3	4	5
Avg. P_{WF} [MW]	275.5	311.5	220.5	324.5	280.0
SD of P_{WF} [MW]	45.5	62.5	69.0	68.0	37.5
Max. $\Delta F(P_{\mathrm{WF}})$ [%]	50.58	44.76	45.49	48.55	39.42

one scenario and Table 3 lists the data of WF output obtained with all scenarios. In Table 3, SD stands for the standard deviation. In the simulation, $\eta = 0.85$ is assumed. The simulation is performed on MATLAB/Simulink 2019b and the simulation period is 3600 s.

A. ANALYSIS OF PARAMETERS IN CONTROLLERS

In this subsection, we determine T in the FLF and $P^{\mathrm{n}}_{\mathrm{H}}$ for the proposed and conventional controllers through scenario simulations. Note that the rated power of the HPS $\hat{P}^{\mathrm{n}}_{\mathrm{H}}$ is estimated by $\eta P^{\mathrm{n}}_{\mathrm{H}}$. Similarly, T_{w} in the method proposed in [16] is also determined by scenario simulations. Note that P_{b} in the proposed coordinated controller is set to $P^{\mathrm{n}}_{\mathrm{H}}$.

First, we investigate T in the FLF and $P^{\mathrm{n}}_{\mathrm{H}}$ for the proposed coordinated controller. Figs. 10a and 10b show the maximum $\Delta F(P_{\mathrm{FLF}})$ vs. T and the maximum $|\Delta\underline{P}_{\mathrm{WF}}|$ vs. T, respectively. [5] It is clear from Figs. 10a and 10b that the HPS with the proposed coordinated controller can sufficiently compensate $\Delta|\underline{P}_{\mathrm{WF}}|$ when $T > 314$ s and $P^{\mathrm{n}}_{\mathrm{H}} > 0.33$ p.u. (the base value is $P^{\mathrm{n}}_{\mathrm{WF}} = 500$ MW in p.u.). It implies that the grid code can be guaranteed when $T > 314$ s and $P^{\mathrm{n}}_{\mathrm{H}} > 0.33$ p.u.

Then, we also investigate T and $P^{\mathrm{n}}_{\mathrm{H}}$ for the method proposed in [11] and [12]. Figs. 11a and 11b show the maximum $\Delta F(P_{\mathrm{g}})$ vs. T and the maximum P_{H} vs. T, respectively. As shown in Fig. 11a, the grid code cannot be satisfied in all scenarios. From Fig. 11b, $P^{\mathrm{n}}_{\mathrm{H}} > 0.37$ p.u. is required.

The method proposed in [16] has three design parameters: T, T_{w} and $P^{\mathrm{n}}_{\mathrm{H}}$. We set $T = 350$ s based on the above analysis. Fig. 12a shows the maximum $\Delta F(P_{\mathrm{g}})$ vs. T_{w}. The method proposed in [16] cannot satisfy the grid code for two scenarios even though T_{w} is large. Although we investigated the results for numerous combinations of T and T_{w} other than Fig. 12a through simulations, the grid code cannot be satisfied. Fig. 12b shows the maximum P_{H} vs. T_{w}. From Fig. 12b, $P^{\mathrm{n}}_{\mathrm{H}} > 0.46$ p.u. is required.

Finally, we list the specification and the parameters of the HPS in Table 4 based on the above analysis and Table 2.

[4]Five hard case scenarios are selected from the available wind speed data for illustration.

[5]In this paper, the maximum $\Delta F(P_{\mathrm{FLF}})$, $\Delta F(P_{\mathrm{g}})$, $|\Delta\underline{P}_{\mathrm{WF}}|$, and P_{H} mean the maximum value in the simulation period 3600 s.

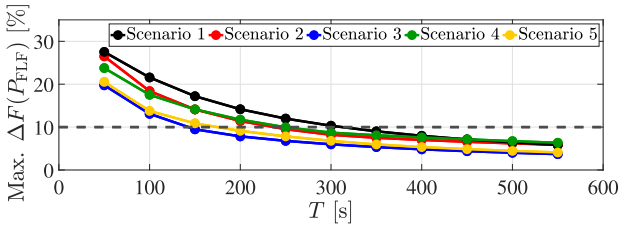

(a)Maximum $\Delta F(P_{\mathrm{FLF}})$ vs. T.

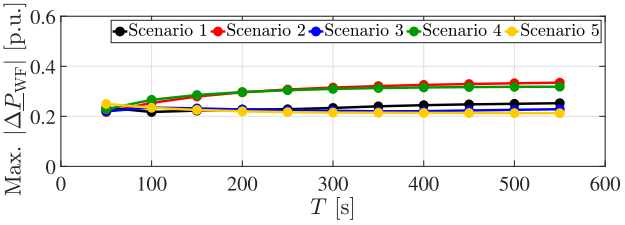

(b)Maximum $|\Delta \underline{P}_{\mathrm{WF}}|$ vs. T.

FIGURE 10. Proposed coordinated controller.

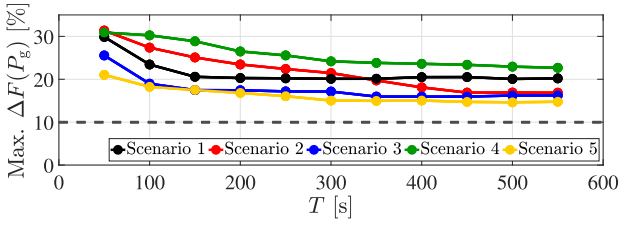

(a)Maximum $\Delta F(P_{\mathrm{g}})$ vs. T.

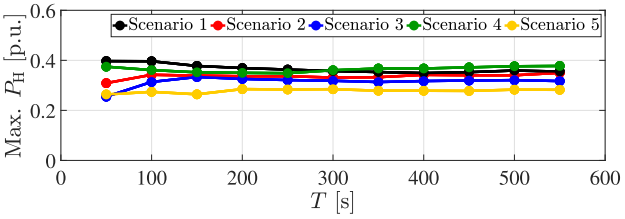

(b)Maximum P_{H} vs. T.

FIGURE 11. Method proposed in [11] and [12].

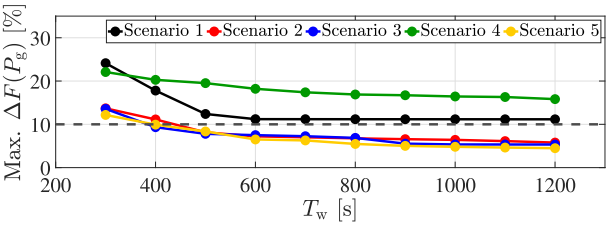

(a)Maximum $\Delta F(P_{\mathrm{g}})$ vs. T_{w} ($T = 350$ s).

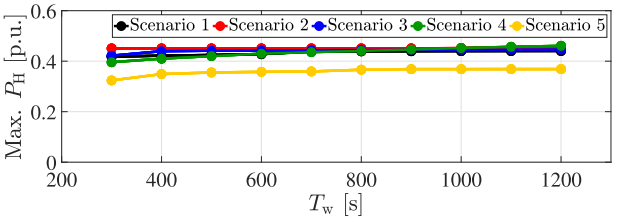

(b)Maximum P_{H} vs. T_{w} ($T = 350$ s).

FIGURE 12. Method proposed in [16].

TABLE 4. Specification of HPS and controller parameters.

	Proposed	[11] and [12]	[16]
Grid code	✓	Unsatisfied	Unsatisfied
$P_{\mathrm{H}}^{\mathrm{n}}$ [MW]	165.9	185.3	233.5
$\hat{P}_{\mathrm{H}}^{\mathrm{n}}(\approx \eta P_{\mathrm{H}}^{\mathrm{n}})$ [MW]	141.0	157.5	198.5
Number of ELZ modules and HPSs $(n_{\mathrm{s}}, n_{\mathrm{p}}, n_{\mathrm{h}})$	64 and 50 $(16, 4, 50)$	84 and 50 $(21, 4, 50)$	90 and 50 $(30, 3, 50)$
H^{n} [Nm^3/h]	24000	31500	33750
R_0 [Ω]	0.12	0.158	0.30
E_0 [V]	1523.2	1999.2	2856
T [s]	350	350	350
T_{w} [s]	–	–	700

The HPS with the conventional controllers cannot satisfy the grid code. Furthermore, the conventional controllers require larger HPS than the proposed coordinated controller.

Note that the parameters of the HPS can be determined in a similar way as above in the real system through measured wind speed data. Moreover, the stability of the system is not affected by the proposed coordinated controller, due to its feed-forward structure as shown in Fig. 7.

B. ANALYSIS OF TIME RESPONSES

In this subsection, we demonstrate the performance of the proposed coordinated controller, comparing it with the conventional methods. Note that the time responses from scenarios 2 to 5 are not included in this paper because of page limitations.

Fig. 13 shows the WF output and the power supplied to the power system. Fig. 14 shows $\Delta F(P_{\mathrm{g}})$. It can be seen from Fig. 13a that the proposed KEC can compensate $\Delta \overline{P}_{\mathrm{WF}}$. In addition, P_{g} obtained with the proposed coordinated controller is similar to $(P_{\mathrm{FLF}} - P_{\mathrm{b}})$. Indeed, the proposed coordinated controller can mitigate the WF output as shown in Fig. 14. In contrast, as shown in Figs. 13b and 13c, P_{g} obtained with the conventional methods include the fluctuation components, compared with P_{FLF}. In particular, as shown in Fig. 13c, the method proposed in [16] causes significant fluctuation in P_{g} when P_{WF} suddenly decreases. As a result, it is difficult for the conventional methods to satisfy the grid code as shown in Fig. 14. Fig. 15 shows the consumed power in the HPS. It is observed from Fig. 15 that the proposed coordinated controller does not require the HPS with high rated power because the HPS with the proposed VDC only compensates $\Delta \underline{P}_{\mathrm{WF}}$. Moreover, the HPS with the proposed VDC operates at around the rated power. As a result, the capacity factor is increased. In contrast, the conventional methods require the HPS with high rated power to compensate the large-output fluctuation of WF instantaneously and operate at low power when $(P_{\mathrm{WF}} - P_{\mathrm{g}}^{\mathrm{ref}})$ is small. Therefore, it is inevitable to decrease the capacity factor. Fig. 16 shows the hydrogen gas produced in the HPS. It is clear that the HPS with the proposed VDC can produce more hydrogen gas than that with the conventional methods.

TABLE 5. Simulation results.

	Scenario 1			Scenario 2			Scenario 3		
	Proposed	[11] and [12]	[16]	Proposed	[11] and [12]	[16]	Proposed	[11] and [12]	[16]
Max. $\Delta F(P_g)$ [%]	9.01	19.73	11.19	7.50	20.12	7.01	5.34	15.96	7.25
Grid code	✓	Unsatisfied	Unsatisfied	✓	Unsatisfied	✓	✓	Unsatisfied	✓
SD of ΔP_g [MW]	14.5	16.5	15.5	23.0	28.5	19.5	16.5	22.0	23.0
Avg. value of P_g [MW]	123.5	235.0	190.0	152.0	265.0	210.0	62.5	182.5	135.0
Hydrogen gas [Nm^3]	20495	5655	12350	21145	6600	14850	21410	5235	12370
Capacity factor [%]	85.4	18.0	36.6	88.1	21.0	44.0	89.2	16.6	36.7

	Scenario 4			Scenario 5			Average		
	Proposed	[11] and [12]	[16]	Proposed	[11] and [12]	[16]	Proposed	[11] and [12]	[16]
Max. $\Delta F(P_g)$ [%]	8.10	23.83	17.4	5.96	14.96	6.28	–	–	–
Grid code	✓	Unsatisfied	Unsatisfied	✓	Unsatisfied	✓	–	–	–
SD of ΔP_g [MW]	15.5	22	24	8	12.5	8	15.5	20.5	18
Avg. value of P_g [MW]	167	275.0	231.5	122.5	243.5	200.0	125.5	240.0	190.0
Hydrogen gas [Nm^3]	20860	6975	13520	21265	5015	11505	21035	5900	12920
Capacity factor [%]	86.9	22.1	40.1	88.6	15.9	34.1	87.6	18.7	38.3

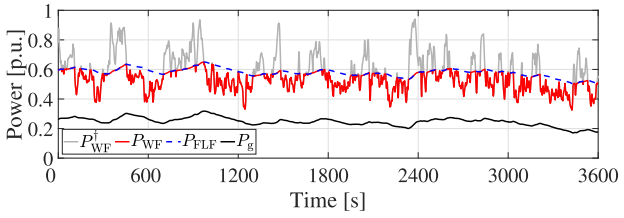

(a)Proposed coordinated controller.

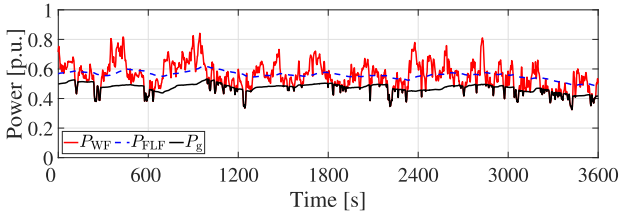

(b)Method proposed in [12] and [11].

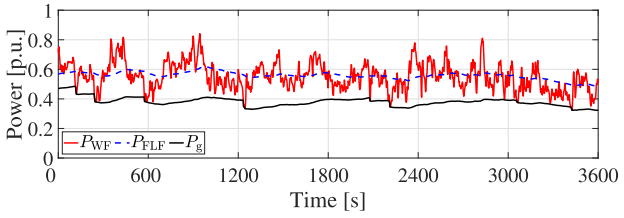

(c)Method proposed in [16].

FIGURE 13. WF output and power supplied to power system.

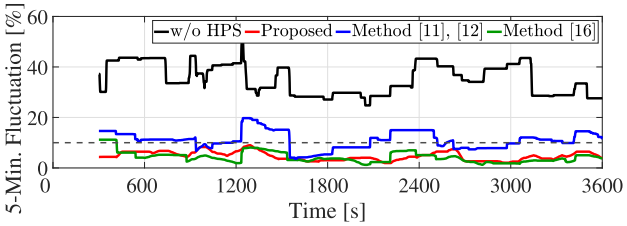

FIGURE 14. $\Delta F(P_g)$.

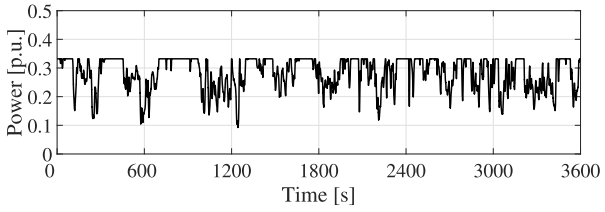

(a)Proposed coordinated controller.

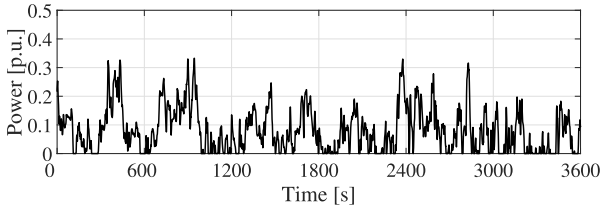

(b)Method proposed in [11] and [12].

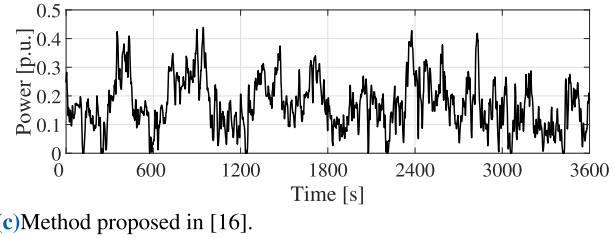

(c)Method proposed in [16].

FIGURE 15. Consumed power in HPS.

Efficiency decrease of the WF is inevitable with a KEC in comparison with the MPPT. As can be seen from Fig. 17, the WF with the proposed KEC operates at a different rotor speed from the WF controlled by the MPPT. It implies that the efficiency in the WF with the proposed KEC also decrease. We investigate the efficiency of the WF with the proposed KEC based on

$$\text{Efficiency} = \frac{\int_0^\tau P_{\text{WF}}}{\int_0^\tau \hat{P}_{\text{WF}}} \times 100\%, \tag{25}$$

where $\hat{P}_{\text{WF}}$ is the WF output obtained by the MPPT. Fig. 18 shows the efficiency vs. T. It can be observed from Fig. 18 that the deterioration of efficiency is about 5% even if T is large.

Table 5 summarizes the simulation results. It contains the average values of all scenarios. Table 6 shows the

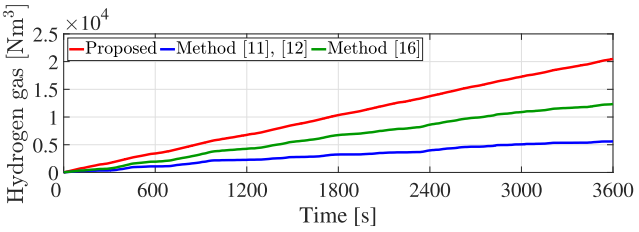

FIGURE 16. Hydrogen gas.

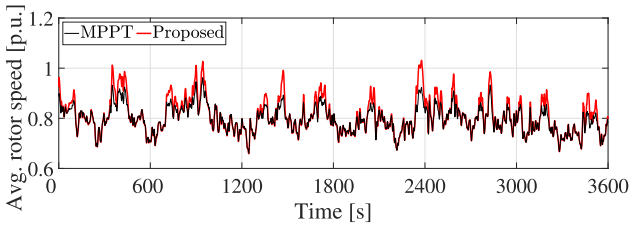

FIGURE 17. Average rotor speed.

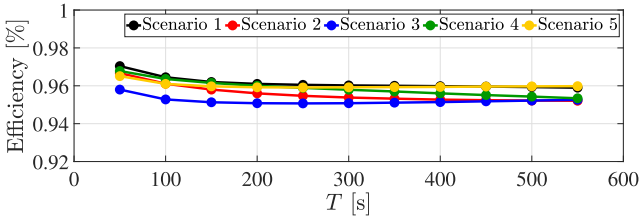

FIGURE 18. Efficiency of WF.

TABLE 6. Performance indices of system.

	Proposed	[11] and [12]	[16]
Avg. value of P_{WF} [MW]	270.0	282.5	282.5
Avg. value of P_{g} [MW]	125.5	240.0	190.0
Power ratio in P_{g}[a]	1	1.91	1.51
$P_{\mathrm{H}}^{\mathrm{n}}$ [MW]	165.9	185.3	233.5
Power ratio in HPS[b]	1	1.12	1.41
Hydrogen gas [Nm^3]	21035	5900	12920
Hydrogen gas ratio[c]	1	0.28	0.61
Capacity factor [%]	87.6	18.7	38.3
Capacity factor ratio[d]	1	0.21	0.44

[a] Power ratio in $P_{\mathrm{g}} = \frac{\text{Avg. value of } P_{\mathrm{g}} \text{ obtained with the conv. controller}}{\text{Avg. value of } P_{\mathrm{g}} \text{ obtained with the pro. controller}}$.
[b] Power ratio in HPS $= \frac{P_{\mathrm{H}}^{\mathrm{n}} \text{ of the HPS with the conv. controller}}{P_{\mathrm{H}}^{\mathrm{n}} \text{ of the HPS with the pro. controller}}$.
[c] Hydrogen gas ratio $= \frac{\text{Hydrogen gas obtained with the conv. controller}}{\text{Hydrogen gas obtained with the pro. controller}}$.
[d] Capacity factor ratio $= \frac{\text{Capacity factor in the HPS with the conv. controller}}{\text{Capacity factor in the HPS with the pro. controller}}$.

performance indices of the system composed of the WF and the HPS through simulation results. Although the average value of P_{g} obtained with the proposed coordinated controller is 47.7% lower than that obtained with the method proposed in [11] and [12] and 34.0% lower than that obtained with the method proposed in [16], the hydrogen gas obtained with the proposed coordinated controller is 72% higher than that obtained with the method proposed in [11] and [12] and 39% higher than that obtained with the method proposed in [16]. Nevertheless, the rated power of HPS is the lowest among the control methods. In particular, the rated power of the HPS with the proposed controller is 29% lower than that with the the method proposed in [16]. As a result, the proposed coordinated controller achieves a capacity factor as high as 87.6% while those of conventional methods are less than 40%.

It is evident from the simulation results that the proposed coordinated controller can mitigate the WF output sufficiently and achieve a high capacity factor in the HPS.

Remark 1: The average value of P_{g} obtained by the proposed coordinated controller is smaller than that obtained by the conventional methods. Nevertheless, the proposed coordinated controller allows us to introduce a large scale WF to power systems because the grid code can be satisfied. This implies that the average value of P_{g} can be increased in the proposed coordinated controller.

V. CONCLUSION

This paper proposed a novel coordinated control method for the system composed of a WF and an HPS. The proposed KEC and VDC could smooth the fluctuation component of the WF sufficiently without increasing the rated power of the HPS. Moreover, the HPS with the proposed controller produced more hydrogen gas while keeping the capacity factor high.

Comparative scenario simulations between the proposed coordinated controller and the conventional controllers demonstrated that the HPS with the proposed coordinated controller could mitigate the WF output fluctuation with a lower HPS rated power and produce hydrogen gas constantly. The simulation results validated that the proposed coordinated controller was more effective than the existing control methods for systems composed of WF and HPS.

In the coordinated control, it is inevitable that the efficiency of the WG degrades. In addition, time-consuming simulations are often needed to design T in the FLF and P_{b}. Future work includes the optimization of WG's efficiency and the parameter design of the coordinated controller.

APPENDIX

We derive (11) and (12) in Appendix. In the following analysis, we assume $V_{\mathrm{dc}} \geq E_0$ and $I_{\mathrm{dc}} > 15.164$ A for simplicity of description.

First, we investigate (11). Substituting $V_{\mathrm{dc}} = \frac{\eta P_{\mathrm{H}}}{I_{\mathrm{dc}}}$ into (8), we obtain

$$R_0 I_{\mathrm{dc}}^2 + E_0 I_0 - \eta P_{\mathrm{H}} = 0. \tag{26}$$

From (26) and $I_{\mathrm{dc}} > 0$, we obtain

$$I_{\mathrm{dc}} = \frac{-E_0 + \sqrt{E_0^2 + 4\eta R_0 P_{\mathrm{H}}}}{2R_0}. \tag{27}$$

As a result, (11) is obtained by substituting (27) into (9).

Then, we derive (12) for large-scale HPSs. Since the consumed power in one of the HPSs connected in parallel is $\left(\frac{P_{\mathrm{H}}}{n_{\mathrm{h}}}\right)$, the current flowing through the cascaded ELZ modules

in a group can be calculated by

$$I_{\mathrm{dc}} = \frac{-E_0 + \sqrt{E_0^2 + 4\eta R_0 \left(\frac{P_{\mathrm{H}}}{n_{\mathrm{h}}}\right)}}{2R_0 n_{\mathrm{p}}}. \tag{28}$$

Let $H^{\ddagger}$ be the hydrogen gas flow rate of one ELZ module involved in the large-scale HPS. From (9) and (28), $H^{\ddagger}$ is given by

$$H^{\ddagger} = 0.019\left(\frac{-E_0 + \sqrt{E_0^2 + 4\eta R_0 \left(\frac{P_{\mathrm{H}}}{n_{\mathrm{h}}}\right)}}{2R_0 n_{\mathrm{p}}}\right) - 0.29. \tag{29}$$

Therefore, the total hydrogen gas flow rate given by (12) is derived by multiplying (29) by $n_{\mathrm{h}} n_{\mathrm{s}} n_{\mathrm{p}}$.

REFERENCES

[1] *Global Wind Report 2021*, Global Wind Energy Council, Brussels, Belgium, 2021.

[2] *Global Offshore Wind Report*, Global Wind Energy Council, Brussels, Belgium, 2020.

[3] K. Yoshimoto, T. Nanahara, and G. Koshimizu, "New control method for regulating state-of- charge of a battery in hybrid wind power/battery energy storage system," in *Proc. IEEE PES Power Syst. Conf. Expo.*, Oct. 2006, pp. 1244–1251.

[4] H. Bevrani, A. Ghosh, and G. Ledwich, "Renewable energy sources and frequency regulation: Survey and new perspectives," *IET Renew. Power Gener.*, vol. 4, no. 5, pp. 438–457, Sep. 2010.

[5] K. Koiwa, T. Ishii, K.-Z. Liu, T. Zanma, and J. Tamura, "On the reduction of the rated power of energy storage system in wind farms," *IEEE Trans. Power Syst.*, vol. 35, no. 4, pp. 2586–2596, Jul. 2020.

[6] M. Jannati, S. H. Hosseinian, B. Vahidi, and G.-J. Li, "Mitigation of wind-farm power fluctuation by adaptive linear neuron-based power tracking method with flexible learning rate," *IET Renew. Power Gener.*, vol. 8, no. 6, pp. 659–669, 2014.

[7] C.-L. Nguyen and H.-H. Lee, "Power management approach to minimize battery capacity in wind energy conversion systems," *IEEE Trans. Ind. Appl.*, vol. 53, no. 5, pp. 4843–4854, Sep. 2017.

[8] D. Lamsal, V. Sreeram, Y. Mishra, and D. Kumar, "Output power smoothing control approaches for wind and photovoltaic generation systems: A review," *Renew. Sustain. Energy Rev.*, vol. 113, Oct. 2019, Art. no. 109245.

[9] F. Zhang, K. Meng, Z. Xu, Z. Dong, L. Zhang, C. Wan, and J. Liang, "Battery ESS planning for wind smoothing via variable-interval reference modulation and self-adaptive SOC control strategy," *IEEE Trans. Sustain. Energy*, vol. 8, no. 2, pp. 695–707, 2017.

[10] A. Sattar, A. Al-Durra, C. Caruana, M. Debouza, and S. M. Muyeen, "Testing the performance of battery energy storage in a wind energy conversion system," *IEEE Trans. Ind. Appl.*, vol. 56, no. 3, pp. 3196–3206, May 2020.

[11] H. Kinoshita, R. Takahashi, T. Murata, J. Tamura, M. Sugimasa, A. Komura, M. Futami, M. Ichinose, and K. Ide, "A study of hydrogen generation with doubly-fed adjustable speed wind generator," *Electr. Eng. Jpn.*, vol. 175, no. 3, pp. 27–36, Feb. 2011.

[12] R. Takahashi, H. Kinoshita, T. Murata, J. Tamura, M. Sugimasa, A. Komura, M. Futami, M. Ichinose, and K. Ide, "Output power smoothing and hydrogen production by using variable speed wind generators," *IEEE Trans. Ind. Electron.*, vol. 57, no. 2, pp. 485–493, Feb. 2010.

[13] L. Sun, G. Wu, Y. Xue, J. Shen, D. Li, and K. Y. Lee, "Coordinated control strategies for fuel cell power plant in a microgrid," *IEEE Trans. Energy Convers.*, vol. 33, no. 1, pp. 1–9, Mar. 2018.

[14] D. Shen, C.-C. Lim, and P. Shi, "Fuzzy model based control for energy management and optimization in fuel cell vehicles," *IEEE Trans. Veh. Technol.*, vol. 69, no. 12, pp. 14674–14688, Dec. 2020.

[15] A. Khalatbarisoltani, M. Kandidayeni, L. Boulon, and X. Hu, "Power allocation strategy based on decentralized convex optimization in modular fuel cell systems for vehicular applications," *IEEE Trans. Veh. Technol.*, vol. 69, no. 12, pp. 14563–14574, Dec. 2020.

[16] A. Takahashi, A. Goto, Y. Machida, and S. Funabiki, "A power smoothing control method for a photovoltaic generation system using a water electrolyzer and its filtering characteristics," *Electr. Eng. Jpn.*, vol. 206, no. 2, pp. 25–32, Oct. 2019.

[17] F. J. Pino, L. Valverde, and F. Rosa, "Influence of wind turbine power curve and electrolyzer operating temperature on hydrogen production in wind–hydrogen systems," *J. Power Sources*, vol. 196, no. 9, pp. 4418–4426, May 2011.

[18] J. Koponen, V. Ruuskanen, A. Kosonen, M. Niemela, and J. Ahola, "Effect of converter topology on the specific energy consumption of alkaline water electrolyzers," *IEEE Trans. Power Electron.*, vol. 34, no. 7, pp. 6171–6182, Jul. 2019.

[19] A. Nelabhotla, D. Pant, and C. Dinamarca, "Chapter 8-power-to-gas for methanation," in *Emerging Technologies and Biological Systems for Biogas Upgrading*, B. Upgrading, N. Aryal, L. D. Ottosen, M. Vedel, W. Kofoed, and D. Pant, Eds. New York, NY, USA: Academic, 2021, pp. 187–221.

[20] K. Koiwa, A. Umemura, R. Takahashi, and J. Tamura, "Stand-alone hydrogen production system composed of wind generators and electrolyzer," in *Proc. 39th Annu. Conf. Ind. Electron. Soc.*, 2013, pp. 1873–1879.

[21] M. Trifkovic, M. Sheikhzadeh, K. Nigim, and P. Daoutidis, "Modeling and control of a renewable hybrid energy system with hydrogen storage," *IEEE Trans. Control Syst. Technol.*, vol. 22, no. 1, pp. 169–179, Jan. 2014.

[22] A. Khalilnejad, A. Sundararajan, and A. I. Sarwat, "Optimal design of hybrid wind/photovoltaic electrolyzer for maximum hydrogen production using imperialist competitive algorithm," *J. Modern Power Syst. Clean Energy*, vol. 6, no. 1, pp. 40–49, Jan. 2018.

[23] F. Alonge, S. M. Collura, F. D'Ippolito, D. Guilbert, M. Luna, and G. Vitale, "Design of a robust controller for DC/DC converter-electrolyzer systems supplied by μ wecss subject to highly fluctuating wind speed," *Control Eng. Pract.*, vol. 98, no. 104383, May 2020.

[24] F. Garcia-Torres and C. Bordons, "Optimal economical schedule of hydrogen-based microgrids with hybrid storage using model predictive control," *IEEE Trans. Ind. Electron.*, vol. 62, no. 8, pp. 5195–5207, Aug. 2015.

[25] H. R. Esmaeilian and R. Fadaeinedjad, "Resolving power quality issues raised by aerodynamic aspects of wind turbine in isolated microgrids using fuel cell/electrolyzer system," *IEEE Trans. Sustain. Energy*, vol. 7, no. 3, pp. 1274–1283, Jul. 2016.

[26] D. F. Recalde Melo and L.-R. Chang-Chien, "Synergistic control between hydrogen storage system and offshore wind farm for grid operation," *IEEE Trans. Sustain. Energy*, vol. 5, no. 1, pp. 18–27, Jan. 2014.

[27] T. Wen, Z. Zhang, X. Lin, Z. Li, C. Chen, and Z. Wang, "Research on modeling and the operation strategy of a hydrogen-battery hybrid energy storage system for flexible wind farm grid-connection," *IEEE Access*, vol. 8, pp. 79347–79356, 2020.

[28] X. Chen, W. Cao, Q. Zhang, S. Hu, and J. Zhang, "Artificial intelligence-aided model predictive control for a grid-tied wind-hydrogen-fuel cell system," *IEEE Access*, vol. 8, pp. 92418–92430, 2020.

[29] X. Wu, H. Li, X. Wang, and W. Zhao, "Cooperative operation for wind turbines and hydrogen fueling stations with on-site hydrogen production," *IEEE Trans. Sustain. Energy*, vol. 11, no. 4, pp. 2775–2789, Oct. 2020.

[30] S. G. Tesfahunegn, Ø. Ulleberg, P. J. S. Vie, and T. M. Undeland, "PV fluctuation balancing using hydrogen storage—A smoothing method for integration of PV generation into the utility grid," *Energy Proc.*, vol. 12, pp. 1015–1022, Mar. 2011.

[31] M. Rosyadi, A. Umemura, R. Takahashi, J. Tamura, N. Uchiyama, and K. Ide, "Simplified model of variable speed wind turbine generator for dynamic simulation analysis," *IEEJ Trans. Power Energy*, vol. 135, no. 9, pp. 538–549, 2015.

[32] M. Rosyadi, S. M. Muyeen, R. Takahashi, and J. Tamura, "New controller design for PMSG based wind generator with LCL-filter considered," in *Proc. 10th Int. Conf. Electr. Mach.*, Sep. 2012, pp. 2112–2118.

[33] S. Shiva Kumar and V. Himabindu, "Hydrogen production by PEM water electrolysis—A review," *Mater. Sci. for Energy Technol.*, vol. 2, no. 3, pp. 442–454, 2019.

[34] V. Leonardo and R. Castro, "Recent developments on hydrogen production technologies: State-of-the-art review with a focus on green-electrolysis," *Appl. Sci.*, vol. 11, no. 23, p. 11363, 2021.

[35] A. M. Abomazid, N. El-Taweel, and H. E. Farag, "Novel analytical approach for parameters identification of PEM electrolyzer," *IEEE Trans. Ind. Informat.*, early access, Dec. 7, 2021, doi: 10.1109/TII.2021.3132941.

[36] H. Jun and I. Tatsuhiko, "A high-purity hydrogen and oxygen generator (HHOG) for chemical industry," *Tech. Doc. Shinkou Pantetuku*, vol. 40, no. 2, pp. 48–56, Mar. 1997.
[37] A. M. Howlader, N. Urasaki, A. Pratap, T. Senjyu, and A. Y. Saber, "A fuzzy control strategy for power smoothing and grid dynamic response enrichment of a grid-connected wind energy conversion system," *Wind Energy*, vol. 17, no. 9, pp. 1347–1363, Sep. 2014.
[38] S. G. Varzaneh, G. B. Gharehpetian, and M. Abedi, "Output power smoothing of variable speed wind farms using rotor-inertia," *Electr. Power Syst. Res.*, vol. 116, pp. 208–217, Nov. 2014.
[39] K. Koiwa, T. Tawara, M. Watanabe, K.-Z. Liu, T. Zanma, and J. Tamura, "Novel cost reduction method for wind farms associated with energy storage systems by optimal kinetic energy control," *Appl. Sci.*, vol. 10, no. 20, p. 7223, Oct. 2020.
[40] Z. Guo and W. Wu, "Data-driven model predictive control method for wind farms to provide frequency support," *IEEE Trans. Energy Convers.*, early access, Nov. 13, 2021, doi: 10.1109/TEC.2021.3125369.
[41] Kansai Electric Power Company. *Grid Interconnection Technical Requirement*. Accessed: Jan. 16, 2022. [Online]. Available: https://www.kansai-td.co.jp/consignment/agreement/pdf/202201_ktrenkei_dt.pdf

KENTA KOIWA (Member, IEEE) was born in 1989. He received the B.E. and M.E. degrees in electrical engineering from the Kitami Institute of Technology, Japan, in 2012 and 2014, respectively, and the Ph.D. degree in electrical engineering from Chiba University, Japan, in 2017.

Since 2017, he has been an Assistant Professor with the Department of Electrical and Electronic Engineering, Chiba University. His research interests include power systems, renewable energy, and power electronics.

LINMAN CUI received the B.E. degree in electrical engineering from the China University of Petroleum, Qingdao, China, in 2016. She is currently pursuing the M.E. degree in electrical engineering with Chiba University, Japan.

Her research interest includes wind power output smoothing.

TADANAO ZANMA (Member, IEEE) was born in 1972. He received the B.S., M.S., and Dr. Eng. degrees from Nagoya University, in 1995, 1997, and 2000, respectively, all in electrical engineering.

From 2000 to 2007, he was with Mie University initially as a Research Associate. Since 2007, he has been an Assistant Professor. In 2007, he was an Academic Guest at ETH Zürich. He was an Associate Professor with Mie University, from 2009 to 2011. He has been with Chiba University as an Associate Professor, since 2011. His current research interests include hybrid dynamical control, switched systems, networked control systems, especially, system control based on mixed logical dynamical systems and model predictive control.

Dr. Zanma has received FANUC FA and Robot Foundation thesis prize, in 2009, and the IEEJ Distinguished Paper Award, in 2010 and 2015.

KANG-ZHI LIU (Senior Member, IEEE) received the B.E. degree in aeronautic engineering from Northwestern Polytechnical University, China, in 1984, and the M.E. and Ph.D. degrees in electrical engineering from Chiba University, Chiba, Japan, in 1988 and 1991, respectively.

Then, he joined Chiba University and is currently a Professor. He has authored six books. His research interests include control theory, power systems, smart grids, and electrical drives.

Dr. Liu was a recipient of the Young Author Award and three Best Paper Awards from the Society of Instrument and Control Engineers (SICE), Japan. He was the Director and the Executive Director of SICE, in 2017 and 2018, respectively.

JUNJI TAMURA (Senior Member, IEEE) received the B.Sc. (Eng.) degree in electrical engineering from the Muroran Institute of Technology, Japan, in 1979, and the M.Sc. (Eng.) and Dr. Eng. degrees in electrical engineering from Hokkaido University, Japan, in 1981 and 1984, respectively.

He became a Lecturer, in 1984, an Associate Professor, in 1986, and a Professor, in 1996, with the Kitami Institute of Technology, Japan.